

# Constraints on the Sommerfeld-enhanced dark matter annihilation from the gamma rays of subhalos and dwarf galaxies

Bo-Qiang Lu,<sup>a</sup> Yue-Liang Wu,<sup>a,b</sup> Wei-Hong Zhang<sup>a,b</sup> and Yu-Feng Zhou<sup>a,b</sup>

<sup>a</sup>State Key Laboratory of Theoretical Physics, Institute of Theoretical Physics, Chinese Academy of Sciences Beijing, 100190, P.R. China

<sup>b</sup>University of Chinese Academy of Sciences, Beijing, 100049, P.R. China

E-mail: [bqlu@itp.ac.cn](mailto:bqlu@itp.ac.cn), [ylwu@itp.ac.cn](mailto:ylwu@itp.ac.cn), [whzhang@itp.ac.cn](mailto:whzhang@itp.ac.cn), [yfzhou@itp.ac.cn](mailto:yfzhou@itp.ac.cn)

**Abstract.** The substructures of the Galactic dark matter halo such as dark matter subhalos and dwarf galaxies have very low velocity dispersions, which makes them useful in constraining the scenario of Sommerfeld-enhanced dark matter annihilation. We calculate the velocity distribution of dark matter particles in dark matter halo substructures using the Eddington's formula with NFW density profile. We parametrize the effect of Sommerfeld enhancement of  $s$ -wave dark matter annihilation on the gamma-ray flux as the Sommerfeld-enhanced J-factors, and explicitly calculate their values for 15 known dwarf spheroidal galaxies. Using the Fermi-LAT 3FGL data on the unassociated point-sources and the N-body simulation results on the dark matter subhalo distribution, we derive upper limits on the dark matter annihilation cross sections with Sommerfeld enhancement. Similar upper limits are derived from the Fermi-LAT gamma-ray data on the dwarf spheroidal galaxies. We find that in a wide region of parameter space, the constraints can be a few orders of magnitude more stringent than that in the case without the Sommerfeld enhancement. For dark matter annihilation dominantly into  $e^+e^-$ ,  $\mu^+\mu^-$ ,  $\tau^+\tau^-$  and  $b\bar{b}$ , those constraints can exclude thermal relic dark matter for the dark matter mass below about 1 TeV.

**Keywords:** dark matter, gamma-ray, Sommerfeld enhancement, velocity distribution

---

## Contents

|          |  |           |
|----------|--|-----------|
| <b>1</b> | <b>Introduction</b>  | <b>1</b>  |
| <b>2</b> | <b>Dark matter velocity distribution function</b>                    | <b>2</b>  |
| 2.1      | Eddington’s formula  | 2         |
| 2.2      | Dark matter profile  | 4         |
| <b>3</b> | <b>Sommerfeld enhancement</b>  | <b>5</b>  |
| <b>4</b> | <b>Sommerfeld-enhanced J-factor</b>                                  | <b>6</b>  |
| <b>5</b> | <b>Constraints from the Fermi-LAT gamma-ray sources observations</b> | <b>8</b>  |
| 5.1      | Constraints from the Fermi-LAT subhalo searches                      | 8         |
| 5.2      | Constraints from the Fermi-LAT dSphs searches                        | 11        |
| <b>6</b> | <b>Summary</b>   | <b>13</b> |
| <b>A</b> | <b>Dimensionless velocity distribution function</b>                  | <b>15</b> |
| <b>B</b> | <b>Analytic solutions for the Sommerfeld enhancement</b>             | <b>16</b> |

---

## 1 Introduction

Cosmological and astrophysical observations have shown that about 85% of the matter in the Universe consists of cold dark matter (DM) rather than Standard Model (SM) particles [1–3]. The most popular class of dark matter particle candidates is that of weakly interacting massive particles (WIMPs) [4, 5]. These particles decouple from the thermal bath as the early Universe expanding and cooling and finally achieve the appropriate relic density. In this scenario, the observed dark matter abundance determines the dark matter annihilation cross-section, provided that the dark matter particles are massive enough to have become non-relativistic at freeze-out. The particles such as high energy gamma rays, pairs of electrons and positrons and antiprotons produced in the annihilation of dark matter in regions of high dark matter density [6, 7], including the Galactic center [8–10], subhalos in the Milky Way [11, 12], and dark matter mini-spikes around intermediate-mass black holes provide a valuable chance to study the nature of dark matter indirectly through accurate measurements of cosmic-rays spectra [13–15].

Small matter density perturbations in the early Universe grow via gravitational instability giving rise to cold, collisionless dark matter bound structures known as halos. N-body simulations under the standard  $\Lambda$ CDM cosmological framework demonstrate that dark matter halos form hierarchically [16], with low-mass halos forming first and then large-mass halos resulting from the merging and accretion of those smaller halos. The hierarchical nature of the structure formation implies that halos contain very large numbers of smaller subhalos, which orbit within the potential well of a more massive host halo [17, 18]. Subhalos can play a crucial role for indirect dark matter searches, since the cosmic-rays flux produced from the self-annihilation of dark matter is proportional to the square of the dark matter density and

hence, the presence of substructure could lead to an enhancement over the expected signal from the smooth distribution of dark matter in the host halo [19].

Under the assumption that the dark matter annihilation cross section (the cross section multiply by the velocity) is velocity-independent, the gamma-ray flux from the annihilation of dark matter in a subhalo can be expressed as a product of the line-of-sight integral of the dark matter distribution in a subhalo, i.e., the J-factor and a component depending on the particle physics model for dark matter annihilation [20]. In this case, the J-factor is independent of the underlying dark matter particle physics such as the dark matter mass and cross section, thus, the J-factor can be simply factorized from the particle physics. However, in generic cases the dark matter cross section can be velocity-dependent, for instance, in some models the dark matter annihilation cross section is p-wave suppressed (i.e.,  $\sigma v \propto v^2$ ) [21–26]. Furthermore, it has been shown that the dark matter annihilation cross section may be enhanced at low relative velocities by the so-called Sommerfeld enhancement, which results from the exchange of light mediators between dark matter particles [27–38]. The Sommerfeld enhancement provides a physical mechanism for the dark matter explanation of the rising positron fraction at energies  $\gtrsim 10$  GeV observed by the PAMELA and AMS-02 experiments [39–47]. When the annihilation is velocity-dependent, the produced cosmic-ray flux is also affected by the distribution of dark matter particle velocities, which depends on the location in the subhalo, thus the dark matter annihilation cross section cannot be extracted from the J-factor directly [48, 49].

In this work we focus on the dark matter annihilation cross section that is enhanced by the Sommerfeld effect. We determine the so-called Sommerfeld-enhanced J-factor and put constraints on the particle parameter space using the null results from the Fermi-LAT experiment observing on the gamma-ray sources. To this end, in section 2 we firstly make a brief review of the Eddington’s formula. Using this formula, we can determine the dark matter velocity distribution in a subhalo for a given dark matter density profile, with the assumption that the orbits of dark matter particles are isotropic. We define a dimensionless dark matter velocity distribution function and show that this distribution function can be well fitted by an exponential form of velocity. In section 3, we give a study on the Sommerfeld enhancement and the Sommerfeld-enhanced J-factor is presented in section 4. Finally, we take advantage of the Fermi-LAT dark matter searches from gamma-ray sources to put limits on the Sommerfeld enhancement in section 5. For the subhalo observations, we count the number of sources that may be observed by the Fermi-LAT experiment and use this to determine the 95% confidence level Poisson upper limit on the predicted number of such sources. For the dwarf satellite galaxies searches, we perform the analysis and use the likelihood function provided by the Fermi Collaboration to determine the upper limits on the dark matter parameters space at 95% confidence level. With these results, we show that the Sommerfeld enhancement parameter spaces that may account for the positron anomaly have been excluded by the Fermi-LAT gamma-ray observation results. In section 6, we summarize our conclusions.

## 2 Dark matter velocity distribution function

### 2.1 Eddington’s formula

For the purpose of determination the velocity distribution of dark matter, we assume that the gravitational potential of dark matter bound states are spherically-symmetric and the orbits of dark matter particles are isotropic. Simulation studies of the velocity anisotropy profiles of dark matter subhalos are consistent with this range out to the subhalo virial radius

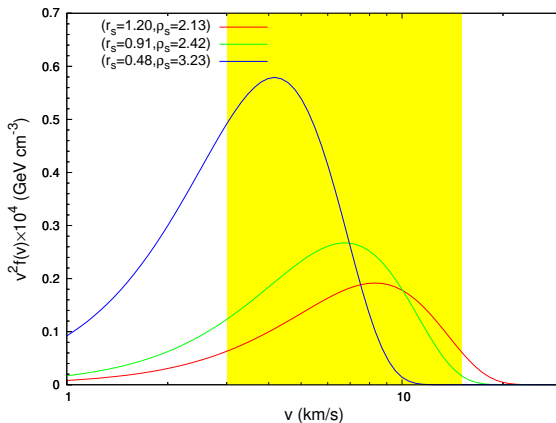


**Figure 1.** Plots of  $v^2 f(v)$  as a function of velocity, evaluated at radius  $r = 0.5r_s$ .  $r_s$  is in unit kpc and  $\rho_s$  is in unit  $\text{GeV cm}^{-3}$ . The yellow band stands for the velocity of dark matter particle in (3 – 15) km/s, which is a typical velocity range of the dwarf galaxy given by the measurements [52].

[49, 50]. With these assumptions, the particle velocity distribution function can be uniquely determined using the Eddington’s formula [51] for a given mass density profile  $\rho(r)$

$$f(\varepsilon) = \frac{1}{\sqrt{8\pi^2}} \int_{\varepsilon}^0 \frac{d^2\rho}{d\Psi^2} \frac{d\Psi}{\sqrt{\Psi - \varepsilon}}. \quad (2.1)$$

where  $\Psi(r)$  represents the spherically-symmetric gravitational potential at position  $r$ ,  $f(\varepsilon) \equiv f(r, v)$  is the dark matter velocity distribution function,  $v$  is dark matter particle velocity (in unit c) and  $\varepsilon = v^2/2 + \Psi(r) < 0$  is the gravitational binding energy per mass of a dark matter particle. The dark matter density profile and velocity distribution function satisfy the normalization  $\rho(r) = \int f(r, v) d^3\vec{v}$ . For an isotropic velocity distribution function  $f(r, v)$ , this can be written as

$$\rho(r) = 4\pi \int_0^{v_{\text{esc}}} v^2 f(r, v) dv, \quad (2.2)$$

with  $v_{\text{esc}} = \sqrt{-2\Psi(r)}$  is the escape velocity of a dark matter particle at radius  $r$  in the gravitational binding system.

The dark matter distribution function  $f(r, v)$  depends only on the parameters  $(r_s, \rho_s)$  of the dark matter profile. In Figure 1, we plot the  $v^2 f(r, v)$  at radius  $r = 0.5r_s$  as a function of dark matter particle velocity. The red, green and blue line stand for the function  $v^2 f(r, v)$  with parameters (1.20 kpc, 2.13  $\text{GeV cm}^{-3}$ ), (0.91 kpc, 2.42  $\text{GeV cm}^{-3}$ ) and (0.48 kpc, 3.23  $\text{GeV cm}^{-3}$ ). These parameters are corresponding to the typical dwarf spheroidal galaxies mass scales. The measurements of the dwarf galaxy stellar velocity dispersion profiles show that the velocity typically span 3 to 15 km/s [52], this is represented by the yellow band in the figure.

The distribution function  $f(r, v)$  can be expressed as a product of a dimensionless distribution function and a scale factor, we find that the dimensionless velocity distribution function can be parameterized by an exponential form of velocity. We show these in detail in the Appendix A.

## 2.2 Dark matter profile

In this work, the Navarro-Frenk-White (NFW) profile is used to approximate the dark matter density distribution [53]

$$\rho(r) = \frac{\rho_s}{(r/r_s)(1+r/r_s)^2}, \quad (2.3)$$

with  $r_s$  and  $\rho_s$  are the scale radius and density of the dark matter distribution profile.

For the subhalos we concerned in this work, the scale parameters  $r_s$  and  $\rho_s$  are uniquely defined for each subhalo from the values of  $V_{\max}$  and  $R_{V_{\max}}$  with the relations

$$r_s = \frac{R_{V_{\max}}}{2.163} \quad (2.4)$$

$$\rho_s = \frac{4.625}{4\pi G} \left( \frac{V_{\max}}{r_s} \right)^2, \quad (2.5)$$

where  $r_s$  is in kpc,  $V_{\max}$  and  $R_{V_{\max}}$  are the maximum circular velocity and the radius of maximum circular velocity. Fitting to the Via Lactea II simulation data shows that the relations between  $V_{\max}$ ,  $R_{V_{\max}}$  and the subhalo masses  $M$  can be parameterized as [20]

$$V_{\max} = V_0 \left( \frac{M}{M_\odot} \right)^\beta \quad (2.6)$$

$$R_{V_{\max}} = R_0 \left( \frac{M}{M_\odot} \right)^\delta, \quad (2.7)$$

where  $V_0 = 10^{-1.20 \pm 0.05} \text{ km s}^{-1}$ ,  $\beta = 0.30 \pm 0.01$  and  $R_0 = 10^{-3.1 \pm 0.4} \text{ kpc}$  and  $\delta = 0.39 \pm 0.02$ , with a log-normal scatter  $\sigma_{V_{\max}} = 0.063 \text{ km s}^{-1}$  and  $\sigma_{R_{V_{\max}}} = 0.136 \text{ kpc}$  for each fitting equation.

We notice that although under the framework of  $\Lambda$ CDM cosmology, large N-body numerical simulations lead to the commonly used NFW halo cuspy spatial density profile, analysis of observations in the central regions of various dwarf halos is in favor of cored profiles, which are much flatter than cusp profiles [18, 54–56]. The self-interacting dark matter scenario may provide one of the possible solutions to this problem [57]. In this scenario, scattering between dark matter particles is more prevalent in the halo center where the dark matter density is largest. Thus in these regions dark matter density distribution may alter by the dark matter self-interaction and tend to deviate from the standard NFW profile. To take the self-interaction into account, a two-region dark matter density profile was proposed in Ref. [58]

$$\rho(r) = \begin{cases} \rho_{\text{NFW}}(r) & \text{if } r > r_1 \\ \rho_{\text{iso}}(r) & \text{if } r < r_1 \end{cases} \quad (2.8)$$

where  $\rho_{\text{iso}}(r)$  is the isothermal profile, the characteristic radius  $r_1$  is determined with the relation  $\frac{\langle \sigma v \rangle}{m} \rho(r_1) t_{\text{age}} \simeq 1$ , where  $t_{\text{age}}$  is the age of a halo. The dark matter density profile is expected to be the NFW profile in the regions  $r > r_1$ , in which scattering has occurred less than once per particle on average. In the halo center at radius  $r < r_1$ , scattering has occurred more than once per particle, and the behavior of dark matter particle is expected to be like the ideal isothermal gas. The density profile of the isothermal gas can be obtained by solving

the equation  $\sigma_0^2 \Delta^2 \ln \rho = -4\pi G \rho$ , where  $\sigma_0$  is the one-dimensional velocity dispersion. This leads to a flat dark matter density profile in the center region of the halo, i.e.,  $\rho(r < r_1) \simeq \rho_{\text{NFW}}(r = r_1)$  (for this research, the reader may see the Refs. [58–60] for more detail). With these results, we thus make a cutoff in the NFW density profile in consideration of the dark matter self-interaction. This is in accordance with the method mentioned above to a large extent.

### 3 Sommerfeld enhancement

The ‘‘Sommerfeld enhancement’’ is the effect that enhances the dark matter annihilation cross sections in the low-velocity regime, this nonrelativistic quantum effect arises due to the formation of long range attractive interaction. If the dark matter particles interact via the exchange of some kind of light mediator, their incoming wave function can be distorted by the presence of a long range potential when their kinetic energy is low enough [28, 35]. In view of the quantum field theory, the Sommerfeld effect corresponds to the contribution of ‘‘ladder’’ Feynman diagrams like the one shown in Figure 2 in which the force carrier is exchanged many times before the annihilation finally occurs. This process gives rise to nonperturbative corrections to the annihilation cross section of dark matter [61].

We consider a hidden sector in which the dark matter particle  $\chi$  couple to a light force carrier  $\phi$  with coupling  $g_X = \sqrt{4\pi\alpha_X}$ . The actual annihilation cross section times relative velocity is  $(\sigma_{\text{ann}}v_{\text{rel}}) = (\sigma_{\text{ann}}v_{\text{rel}})_0 \times S$ , where  $(\sigma_{\text{ann}}v_{\text{rel}})_0$  is the tree-level cross section times relative velocity and  $S$  stands for the Sommerfeld enhancement. We assume that the dark matter tree-level annihilation cross section is dominated by s-wave processes, which is unsuppressed at low velocities. Let  $\psi(r)$  be the reduced two-body wave function for the s-wave annihilation, in the nonrelativistic limit, the motion of the reduced two-body wavefunction obeys the radial Schrödinger equation

$$\frac{1}{m_\chi} \frac{d^2\psi}{dr^2} - V(r)\psi(r) = -m_\chi v^2 \psi(r), \quad (3.1)$$

where  $m_\chi$  is the dark matter mass and  $v = v_{\text{rel}}/2$  is the velocity of each particle in the center-of-mass frame. The attractive force between nonrelativistic dark matter particles mediated by a scalar or vector is described by a Yukawa potential

$$V(r) = -\frac{\alpha_X}{r} e^{-m_\phi r}, \quad (3.2)$$

where  $m_\phi$  is the mass of light mediator. The Sommerfeld enhancement  $S$  can be calculated by solving the Schrödinger equation with the boundary condition  $\psi'(r) = im_\chi v \psi(r)$  and  $\psi(r) = e^{im_\chi v r}$  as  $r \rightarrow \infty$ . The Sommerfeld enhancement factor is given by

$$S = \left| \frac{\psi(\infty)}{\psi(0)} \right|^2. \quad (3.3)$$

Defining two dimensionless parameters

$$\varepsilon_v = \frac{v}{\alpha_X} \quad \text{and} \quad \varepsilon_\phi = \frac{m_\phi}{\alpha_X m_\chi}. \quad (3.4)$$

Using the dimensionless variable  $x = \alpha_X m_\chi r$  the radial Schrödinger equation can be rewritten as

$$\psi''(x) + [\varepsilon_v^2 + V(x)]\psi(x) = 0, \quad (3.5)$$

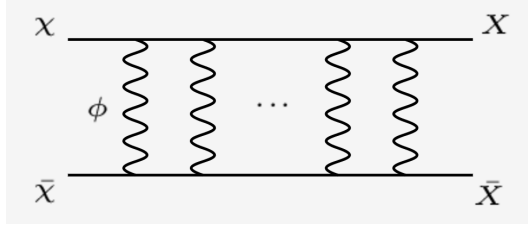


**Figure 2.** Feynman diagram giving rise to the Sommerfeld enhancement for  $\chi\bar{\chi} \rightarrow X\bar{X}$  annihilation processes, wave line stands for the exchange of a light mediator.

with the potential  $V(x) = \exp(-\varepsilon_\phi x)/x$ . The boundary conditions become  $\psi'(x) = i\varepsilon_v\psi(x)$  and  $\psi(x) = \exp(i\varepsilon_v x)$  as  $x \rightarrow \infty$ . Approximating the Yukawa potential as the Hulthén potential we can obtain an analytic formula for Sommerfeld enhancement [62, 63]

$$S = \frac{\pi}{\varepsilon_v} \frac{\sinh\left(\frac{2\pi\varepsilon_v}{\pi^2\varepsilon_\phi/6}\right)}{\cosh\left(\frac{2\pi\varepsilon_v}{\pi^2\varepsilon_\phi/6}\right) - \cos\left(2\pi\sqrt{\frac{1}{\pi^2\varepsilon_\phi/6} - \frac{\varepsilon_v^2}{(\pi^2\varepsilon_\phi/6)^2}}\right)}. \quad (3.6)$$

We show the numerical and analytic results for the Sommerfeld enhancement in the Appendix B.

#### 4 Sommerfeld-enhanced J-factor

The commonly used differential photon flux produced from the annihilation of astrophysical dark matter is given by

$$\frac{d\Phi}{dE_\gamma} = \frac{1}{4\pi} \frac{(\sigma_{\text{ann}}v_{\text{rel}})_0}{2m_\chi^2} \frac{dN}{dE_\gamma} \times \int_{\Delta\Omega} d\Omega \int_{\text{LOS}} dl \rho_\chi^2[r(D, l, \theta)] \quad (4.1)$$

$$= \frac{1}{4\pi} \frac{(\sigma_{\text{ann}}v_{\text{rel}})_0}{2m_\chi^2} \frac{dN}{dE_\gamma} \times J, \quad (4.2)$$

where  $D$  is the distance to the satellite center,  $l$  is the distance along the line of sight,  $\theta$  is the offset angle relative to the center and  $r(D, l, \theta) = \sqrt{D^2 + l^2 - 2Dl \cos\theta}$  is the distance from the satellite center. The angular integration is performed over  $\Delta\Omega = 2\pi(1 - \cos\theta)$ .  $dN/dE_\gamma$  is the photon spectrum produced by a single annihilation process and  $(\sigma_{\text{ann}}v_{\text{rel}})_0$  is the dark matter annihilation cross section. The second term in eq.(4.1) is often called J-factor that encapsulate all astrophysical information for determining the photon flux from dark matter annihilation.

Notice that the annihilation cross section is velocity-independent has been assumed to obtain the differential photon flux eq.(4.1), thus the J-factor is simply an integral over the line-of-sight and over a given angular region of the square of the dark matter density profile of the satellite. This is reasonable for the most discussed neutralino models featuring a mostly s-wave velocity-independent cross section. However, theoretically, the annihilation cross section may be velocity-dependent. Models with p-wave suppressed dark matter annihilation have been studied in many works recently [22, 24, 26, 64]. Velocity-dependent cross section also exists in the dark matter scenarios with Sommerfeld enhancement that have been recently discussed to account for the observed positron cosmic-ray anomalies [28, 29, 31, 35, 36, 41]. In these cases, the J-factor cannot be simply factorized from the particle physics, since

the photon flux arising from dark matter annihilation depends on the dark matter velocity distribution. A generally form of differential photon flux produced from dark matter with a velocity-dependent annihilation cross section can be written as

$$\frac{d\Phi}{dE_\gamma} = \frac{1}{4\pi} \frac{1}{2m_\chi^2} \frac{dN}{dE_\gamma} \times \int_{\Delta\Omega} d\Omega \int_{\text{LOS}} dl \int d^3\vec{v}_1 f(r, \vec{v}_1) \int d^3\vec{v}_2 f(r, \vec{v}_2) (\sigma_{\text{ann}} v_{\text{rel}}). \quad (4.3)$$

In this formula, the annihilation cross section ( $\sigma_{\text{ann}} v_{\text{rel}}$ ) may be p-wave suppressed or Sommerfeld-enhanced. Herein we only take into account the Sommerfeld enhancement and assume that the tree-level dark matter annihilation is dominant by s-wave process. As mentioned above, the Sommerfeld-enhanced annihilation cross section can be expressed as  $(\sigma_{\text{ann}} v_{\text{rel}}) = (\sigma_{\text{ann}} v_{\text{rel}})_0 \times S(v_{\text{rel}}/2)$ , where the tree-level cross section  $(\sigma_{\text{ann}} v_{\text{rel}})_0$  is s-wave dominant, i.e., velocity-independent. Then the eq.(4.3) can be rewritten as

$$\frac{d\Phi}{dE_\gamma} = \frac{1}{4\pi} \frac{(\sigma_{\text{ann}} v_{\text{rel}})_0}{2m_\chi^2} \frac{dN}{dE_\gamma} \times J_S, \quad (4.4)$$

where  $J_S$  is the Sommerfeld-enhanced J-factor which is characteristic by a superscript  $S$  [49]

$$J_S = \int_{\Delta\Omega} d\Omega \int_{\text{LOS}} dl \int d^3\vec{v}_1 f(r, \vec{v}_1) \int d^3\vec{v}_2 f(r, \vec{v}_2) S(|\vec{v}_2 - \vec{v}_1|/2) \quad (4.5)$$

$$\simeq \frac{1}{D^2} \int dV \int d^3\vec{v}_1 f(r, \vec{v}_1) \int d^3\vec{v}_2 f(r, \vec{v}_2) S(|\vec{v}_2 - \vec{v}_1|/2). \quad (4.6)$$

In the limit  $S \rightarrow 1$  (i.e.,  $\varepsilon_\phi \gg 1$ ), we have  $J_S \rightarrow J$ . The Sommerfeld-enhanced J-factor  $J_S$  depends on five parameters, two of them are the particle physics parameters:  $\alpha_X$  and  $\varepsilon_\phi$ , and the other three are astrophysical parameters:  $(r_s, \rho_s)$ , the scales of satellite dark matter profile and  $D$ , the distance to the satellite center.

Notice that the integration of  $J_S$  not only depends on the magnitudes of  $v_1$  and  $v_2$  but also depends on the angle between the velocity of two dark matter particles, we express this explicitly

$$J_S = \frac{32\pi^3}{D^2} \int_0^{r_{\text{max}}} r^2 dr \int_0^{v_{\text{max}}} v_1^2 f(r, v_1) dv_1 \int_0^{v_{\text{max}}} v_2^2 f(r, v_2) dv_2 \times \int_0^\pi \sin\theta S\left(\sqrt{v_1^2 + v_2^2 - 2v_1 v_2 \cos\theta}/2\right) d\theta. \quad (4.7)$$

The  $J_S$  are depicted in Figure 3 as a function of  $\varepsilon_\phi$  with various parameters. The distance  $D$  in the two panels of the figure is assumed to be 50 kpc. In the left panel of Figure 3, we calculate the Sommerfeld-enhanced J-factor for three mass scales of subhalo:  $5 \times 10^6 M_\odot$ ,  $5 \times 10^7 M_\odot$  and  $5 \times 10^8 M_\odot$ , with the coupling  $\alpha_X = 0.01$ . We obtain the scales of dark matter profile  $(r_s, \rho_s)$  for the given subhalo masses using the relations mentioned in the above section, and notice that there are some uncertainties in the fitting equations. In the right panel, we demonstrate the Sommerfeld-enhanced J-factor with various coupling  $\alpha_X$ , assuming  $M = 5 \times 10^7 M_\odot$  and  $D = 50$  kpc. As shown in the figure, the Sommerfeld-enhanced J-factor  $J_S \rightarrow J$  as the  $\varepsilon_\phi$  goes much beyond 1, since in this regions the Sommerfeld enhancement  $S \rightarrow 1$ . The enhanced factor  $J_S/J$  may up to  $\sim 10^3$  for  $\alpha_X = 0.01$  at low  $\varepsilon_\phi$ . The resonances occur at  $\varepsilon_\phi \simeq \frac{6}{\pi^2 n^2}$ , where  $n$  is an integer, and the Sommerfeld enhancement scales as  $\alpha_X^2 \varepsilon_\phi / v^2$ . The resonance amplitude decrease with the increasing of a subhalo mass,



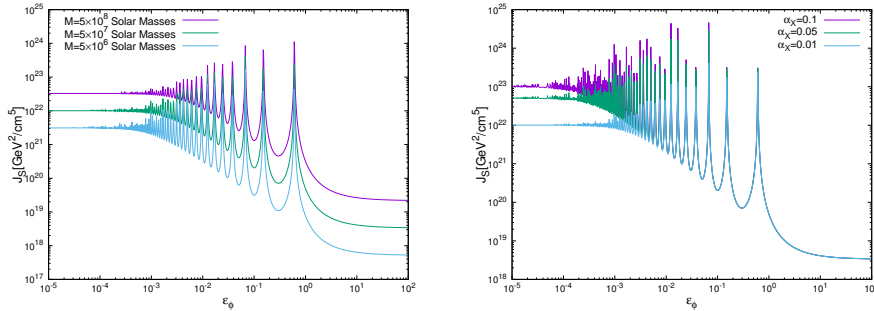


**Figure 3.** Left panel: Sommerfeld-enhanced J-factor as a function of  $\varepsilon_\phi$ , assuming  $D = 50$  kpc and  $\alpha_X = 0.01$ . The purple, green and blue line stand for the results with the subhalo masses  $M = 5 \times 10^8 M_\odot$ ,  $5 \times 10^7 M_\odot$  and  $5 \times 10^6 M_\odot$ . Right panel: Sommerfeld-enhanced J-factor as a function of  $\varepsilon_\phi$ , assuming  $D = 50$  kpc and  $M = 5 \times 10^7 M_\odot$ . The purple, green and blue line represent the results with the  $\alpha_X = 0.1$ ,  $0.05$  and  $0.01$ .

since the average speed of dark matter particles is larger in a much more massive subhalo. The saturation of the Sommerfeld enhancement occurs at about  $\varepsilon_\phi \sim \frac{v}{2\alpha_X}$ , this leads to the constraint  $\varepsilon_\phi \gtrsim 10^{-6}\alpha_X^{-1}$  for the dwarf galaxies, in which the typical dark matter velocity has the scale  $\sim \mathcal{O}(1)$  km/s. As mentioned above, the Sommerfeld enhancement  $S \rightarrow \pi\alpha_X/v$  in the limit  $\varepsilon_\phi \ll \varepsilon_v$  (i.e.,  $\varepsilon_\phi \lesssim 10^{-5}\alpha_X^{-1}$  for the dwarf galaxies). Thus in this region the Sommerfeld-enhanced J-factor is proportional to the coupling  $\alpha_X$ , as is shown in the figure. For the region  $\varepsilon_\phi \gtrsim 10^{-5}\alpha_X^{-1}$ , the Sommerfeld-enhanced J-factor is independent of  $\alpha_X$ .

In order to focus on our topic, we have used the NFW profile and assumed isotropic orbits for the calculation of J-factor. Notice that the previous literatures about the J-factor calculations have allowed for non-NFW profiles, anisotropic stellar velocity dispersions and assumed a Gaussian likelihood for the stellar velocities [52, 65, 66]. Refs. [67, 68] provide a simple analytic formulae to calculate the J-factor for spherical cusp without solving the spherical Jeans equations, which relates the velocities of the stars to the underlying dark matter distribution. In the framework of isotropic orbits, the calculations of non-NFW profiles are analogous, however, it may require to go beyond the Eddington's formula when the anisotropic models are taken into account.

## 5 Constraints from the Fermi-LAT gamma-ray sources observations

### 5.1 Constraints from the Fermi-LAT subhalo searches

Since 2010, The First Fermi-LAT catalog (1FGL) of gamma-ray sources detected by the Large Area Telescope (LAT) was released by the Fermi Collaboration, based on their first 11 months of data. This catalog contains 1451 sources detected and characterized in the 100 MeV to 100 GeV range, 630 of which had (at the time) not been associated with counterparts at other wavelengths [69]. Recently, Bertoni et al. have examined the 3FGL in an effort to identify dark matter subhalo candidates, and to use the population of such sources to constrain the dark matter annihilation cross section. They identified a subset of 24 bright ( $\Phi_\gamma > 7 \times 10^{-10} \text{ cm}^{-2} \text{ s}^{-1}$ ,  $E > 1$  GeV) and high-latitude ( $|b| > 20^\circ$ ) sources that show no evidence of variability and exhibit a spectral shape that is consistent with the predictions of annihilating dark matter [70–73].

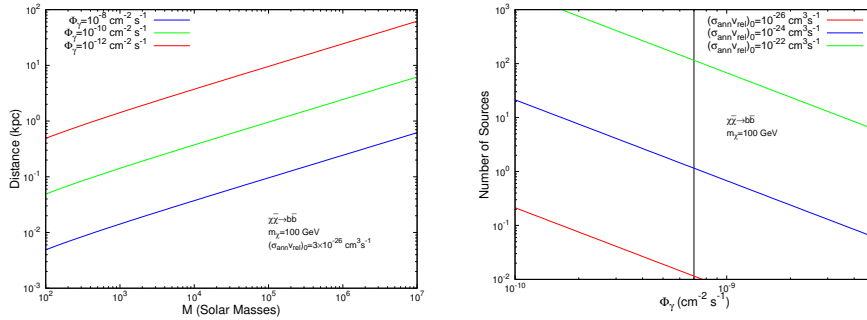


**Figure 4.** Left panel: plots of contours of constant gamma-ray flux in the distances and masses plane, the red, green and blue lines are corresponding to a constant gamma-ray flux of  $10^{-12} \text{ cm}^{-2} \text{ s}^{-1}$ ,  $10^{-10} \text{ cm}^{-2} \text{ s}^{-1}$  and  $10^{-8} \text{ cm}^{-2} \text{ s}^{-1}$  respectively. Right panel: number of gamma-ray sources as a function of  $\Phi_\gamma$ , the red, blue and green line represent the results with  $(\sigma_{\text{ann}} v_{\text{rel}})_0 = 10^{-26}$ ,  $10^{-24}$  and  $10^{-22} \text{ cm}^3 \text{ s}^{-1}$ , the black line stands for  $\Phi_\gamma = \Phi_{\text{threshold}}$ .

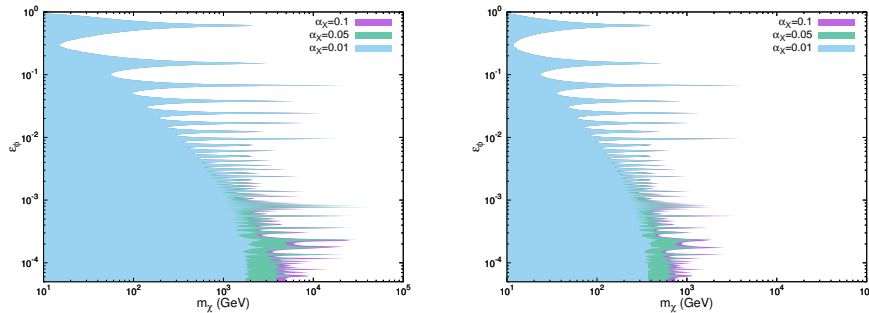


**Figure 5.** The Fermi-LAT subhalo observation results constrain on the  $\epsilon_\phi$  at 95% confidence level. The color shaded parameter space is excluded at 95% confidence level, the dark matter annihilation channel is assumed to be  $b\bar{b}$  and  $\tau\bar{\tau}$  in the left and right panel.

The differential gamma-ray spectrum from dark matter annihilation within an individual subhalo is given by eq.(4.1) for a velocity-independent cross section and eq.(4.3) for a velocity-dependent cross section. For the case of velocity-independent dark matter annihilation cross section, the brightness of the gamma rays from a subhalo mainly depends on the mass and distance of the subhalo and also the density profile of the subhalo. In the left panel of Figure 4, contours of constant gamma-ray flux are shown in the distances and masses plane, and the photon energies are in the range of (1 – 100) GeV. The process considered in the figure is a pair of dark matter annihilate to  $b\bar{b}$  final state, with dark matter mass  $m_\chi = 100 \text{ GeV}$  and a velocity-independent cross section  $(\sigma_{\text{ann}} v_{\text{rel}})_0 = 3 \times 10^{-26} \text{ cm}^3 \text{ s}^{-1}$ . The red, green and blue lines are corresponding to a constant gamma-ray flux of  $10^{-12} \text{ cm}^{-2} \text{ s}^{-1}$ ,  $10^{-10} \text{ cm}^{-2} \text{ s}^{-1}$  and  $10^{-8} \text{ cm}^{-2} \text{ s}^{-1}$  respectively. The high latitude ( $|b| > 10^\circ$ ) subhalo may be observed by Fermi-LAT if the gamma-ray flux produced from these subhalos exceeds the Fermi-LAT experiment threshold (here we take the threshold  $\Phi_{\text{threshold}}$  as that in Ref. [73]). Throughout this work, the dark matter distribution within an individual subhalo is assumed to be the NFW profile, however, we notice that for subhalos located within the innermost few tens of kiloparsecs of their host halo, the distribution of subhalos are significantly altered by tidal effects, and are generally not well described by NFW density profiles, instead preferring power-law profiles with an exponential cutoff [73].

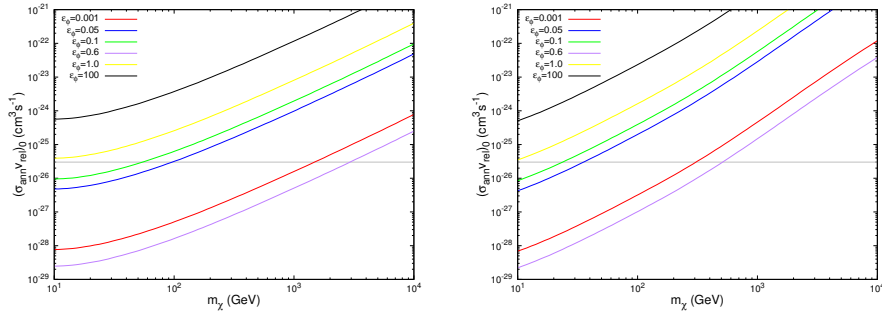


**Figure 6.** Constraints on the dark matter annihilation cross section at 95% confidence level derived from the Fermi-LAT subhalo searches, with a given Sommerfeld-enhanced J-factor. The horizontal grey line stands for a annihilation cross section  $(\sigma_{\text{ann}}v_{\text{rel}})_0 = 3 \times 10^{-26} \text{ cm}^3 \text{ s}^{-1}$ , the dark matter annihilation channel is assumed to be  $b\bar{b}$  and  $\tau\bar{\tau}$  in the left and right panel.

Cosmological simulations show that the mass distribution of subhalo populations follow a power-law form,  $dN/dM \propto M^{-1.9}$  [74, 75]. We make use of the mass distribution for the local subhalo population from Ref. [73], in which the distribution is obtained through fitting to the recently ELVIS simulation data for subhalos with masses between  $10^8 M_\odot$  and  $10^{10} M_\odot$

$$\frac{dN}{dM dV} = \frac{628}{M_\odot \text{kpc}^3} \left( \frac{M}{M_\odot} \right)^{-1.9}. \quad (5.1)$$

A departure from this power-law form arises at lower subhalo masses, this may be due to the finite resolution of the simulation. In this work, the masses of subhalo are assumed to be in the range of  $(10^3 - 10^7) M_\odot$ . For this mass region, more subhalos than the ELVIS simulation results are expected and the power-law form of mass distribution may still be viable [73]. To avoid the inclusion of any dwarf galaxies, the masses of subhalo are restricted below  $10^7 M_\odot$ . There are no observation constraints on the minimum masses of subhalo, the limits on the dark matter annihilation cross section may alter at most 5% – 10% with the variation of the minimum subhalo masses.

With the subhalo mass distribution, the number of subhalos that yield a gamma-ray flux above the Fermi-LAT threshold  $\Phi_{\text{threshold}}$  is given by

$$N_{\text{obs}} = \Omega \int \int \frac{dN}{dM dV} D^2 \Theta(\Phi_\gamma - \Phi_{\text{Thresh}}) dM dD, \quad (5.2)$$

where  $\Theta$  is the step function,  $\Phi_\gamma$  is the gamma-ray flux produced from a subhalo with energies in  $(1 - 100) \text{ GeV}$ , and  $\Omega$  is the solid angle observed by Fermi experiment, which corresponds to  $4\pi(1 - \sin 20^\circ)$  for the case of  $|b| > 20^\circ$ . In the right panel of Figure 4 we plot the number of sources as a function gamma-ray flux produced from the subhalos (here the threshold is not take into account and the dark matter cross section is velocity-independent). The number of sources is proportional to the dark matter annihilation cross section and linearly decrease with the increasing of gamma-ray flux.

With these knowledges, we can put constraints on the Sommerfeld enhancement with the subhalo observations by comparing the number of sources with the number of identified dark matter subhalo candidates. For each choice of  $\varepsilon_\phi$ , we calculate the Sommerfeld-enhanced J-factor (here the dark matter cross section  $(\sigma_{\text{ann}}v_{\text{rel}})_0$  is fixed at  $3 \times 10^{-26} \text{ cm}^3 \text{ s}^{-1}$ ). With eq.(5.2), we count the number of sources that may be observed by the Fermi-LAT experiment

and use this to determine the 95% confidence level (CL) Poisson upper limit on the predicted number of such sources. We then determine the 95% confidence level limits on the parameter  $\varepsilon_\phi$  which corresponds to the Poisson upper limit of the number of sources [76]. In Figure 5, we show the resulting limits on the parameter  $\varepsilon_\phi$  as a function of dark matter mass  $m_\chi$ , for several choices of the coupling  $\alpha_X$ . In the left and right panel of Figure 5, the dark matter annihilation channel is  $b\bar{b}$  and  $\tau\bar{\tau}$  respectively. The color shaded parameter space is excluded at 95% confidence level by the subhalo observations. As shown in the figure, the constraints become more stringent with a larger  $\alpha_X$  for  $\varepsilon_\phi \gtrsim 10^{-3}$ . Our results can be easily changed to the  $m_\phi - m_\chi$  plane by using the relation  $\varepsilon_\phi = m_\phi/(\alpha_X m_\chi)$ .

In Figure 6, we show the constraints on the dark matter annihilation cross section at 95% confidence level as a function of dark matter mass. We assume the coupling  $\alpha_X$  to be 0.1 and determine the Sommerfeld-enhanced J-factor for a given value of  $\varepsilon_\phi$ , we calculate the signal gamma-ray flux from dark matter annihilation for each choice of dark matter mass  $m_\chi$  and annihilation cross section  $(\sigma_{\text{ann}} v_{\text{rel}})_0$ . The same as above, we count the number of sources that may be observed by the Fermi-LAT experiment and determine the 95% confidence level Poisson upper limits on the dark matter annihilation cross section. Although the constraints derived here are somewhat weaker than those based on the observations of dwarf galaxies (see next subsection), the results may be improved with more observations from Fermi-LAT experiments and the future gamma-ray telescopes.

## 5.2 Constraints from the Fermi-LAT dSphs searches

One of the most stringent constraints on the dark matter annihilation cross section to date is the limits from gamma-ray observations of Milky Way dwarf spheroidal satellite galaxies (dSphs). Here we take advantage of the Fermi-LAT dark matter searches from Milky Way dSphs to put limits on the Sommerfeld enhancement. For this purpose, we follow the analysis performed by the Fermi collaboration, which is based on the observation of 15 dwarf galaxies in the energy range 500 MeV – 500 GeV. We perform the statistical analysis using the likelihood in each energy bin as a function of integrated signal flux provided by the Fermi Collaboration [77].

The likelihood function for target dwarf galaxy  $i$  is given by

$$\tilde{\mathcal{L}}_i(\boldsymbol{\mu}, \boldsymbol{\theta}_i = \{\boldsymbol{\alpha}, J_i\} | \mathcal{D}_i) = \mathcal{L}_i(\boldsymbol{\mu}, \boldsymbol{\theta}_i | \mathcal{D}_i) \mathcal{L}_J(J_i | J_{\text{obs},i}, \sigma_i), \quad (5.3)$$

where  $\boldsymbol{\mu}$  are the parameters of the dark matter model (here it is the particular point in the  $(m_\chi, \varepsilon_\phi)$  parameter space under consideration),  $\boldsymbol{\theta}_i$  is the set of nuisance parameters that includes both nuisance parameters from the LAT analysis  $\boldsymbol{\alpha}_i$  and the dSph J-factor  $J_i$ , and  $\mathcal{D}_i$  stands for the gamma-ray data. The J-factor likelihood for target  $i$  can be written as

$$\mathcal{L}_J(J_i | J_{\text{obs},i}, \sigma_i) = \frac{1}{\ln(10) J_{\text{obs},i} \sqrt{2\pi} \sigma_i} \exp(-[\log_{10}(J_i) - \log_{10}(J_{\text{obs},i})]^2 / 2\sigma_i^2), \quad (5.4)$$

where  $J_i$  is the true value of the J-factor and  $J_{\text{obs},i}$  is the measured J-factor with error  $\sigma_i$ . This method allows to take into account the uncertainty on the determination of the J-factors. This correction is only related to the statistical uncertainty in the J-factor [77].

To determine  $\mathcal{L}_i(\boldsymbol{\mu}, \boldsymbol{\theta}_i | \mathcal{D}_i)$ , we compute the dark matter flux in each energy bin and determine the corresponding likelihood for a given point  $\boldsymbol{\mu}$  in the parameter space and choice of  $J_i$ , and then multiply these likelihoods for all the energy bins in the analysis. The total likelihood is obtained through multiplying the J-factor likelihood by the joint likelihood

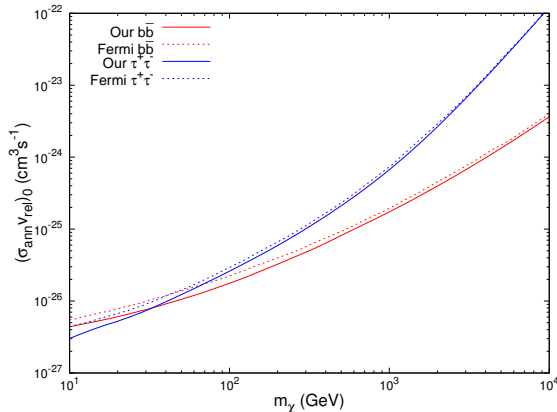


**Figure 7.** Comparison of our calculation results without taking into account the J-factor likelihood (solid lines) with the constraints given by the Fermi Collaboration (dot lines). The red and blue lines represent the results with dark matter annihilation to  $b\bar{b}$  and  $\tau\bar{\tau}$  final state.

**Table 1.** Listing of  $J_S(\varepsilon_\phi)$  and  $J_{\text{obs}}$  for the 15 dSphs.

| Name              | $\log(J_S(1.0))^{ab}$ | $\log(J_S(0.6))^{ab}$ | $\log(J_S(0.1))^{ab}$ | $\log(J_S(0.05))^{ab}$ | $\log(J_{\text{obs}})^b$ |
|-------------------|-----------------------|-----------------------|-----------------------|------------------------|--------------------------|
| Bootes I          | 19.87                 | 23.07                 | 20.48                 | 20.78                  | 18.8                     |
| Canes Venatici II | 18.90                 | 22.10                 | 19.51                 | 19.81                  | 17.9                     |
| Carina            | 19.22                 | 22.42                 | 19.84                 | 20.13                  | 18.1                     |
| Coma Berenices    | 20.03                 | 23.23                 | 20.64                 | 20.94                  | 19.0                     |
| Draco             | 19.95                 | 23.15                 | 20.57                 | 20.86                  | 18.8                     |
| Fornax            | 19.29                 | 22.49                 | 19.91                 | 20.20                  | 18.2                     |
| Hercules          | 19.12                 | 22.32                 | 19.74                 | 20.04                  | 18.1                     |
| Leo II            | 18.60                 | 21.80                 | 19.22                 | 19.51                  | 17.6                     |
| Leo IV            | 18.99                 | 22.19                 | 19.60                 | 19.90                  | 17.9                     |
| Sculptor          | 19.72                 | 22.92                 | 20.33                 | 20.63                  | 18.6                     |
| Segue 1           | 20.61                 | 23.81                 | 21.23                 | 21.52                  | 19.5                     |
| Sextans           | 19.57                 | 22.77                 | 20.18                 | 20.48                  | 18.4                     |
| Ursa Major II     | 20.41                 | 23.61                 | 21.03                 | 21.33                  | 19.3                     |
| Ursa Minor        | 19.94                 | 23.14                 | 20.56                 | 20.85                  | 18.8                     |
| Willman 1         | 20.17                 | 23.37                 | 20.78                 | 21.08                  | 19.1                     |

<sup>a</sup>  $\alpha_X$  is fixed at 0.1.

<sup>b</sup>  $J_S(\varepsilon_\phi)$  and  $J_{\text{obs}}$  in unit  $\text{GeV}^2 \text{cm}^{-5}$ .

$\mathcal{L}_i(\boldsymbol{\mu}, \boldsymbol{\theta}_i | \mathcal{D}_i)$ . The astrophysical parameters ( $V_{\text{max}}, R_{V_{\text{max}}}$ ) for the 15 dSphs are taken from Ref. [65], in which a multilevel statistical modelling technique is used to constrain the dark matter halo properties (this technique is also adopted by the Fermi Collaboration [78]). We then determine the J-factor ( $J_{\text{obs}}$ ) for each dwarf satellite galaxy and find that these results are in good agreement with the values given by the Fermi Collaboration [77]. We show the calculation results of Sommerfeld enhanced J-factor  $J_S$  with various  $\varepsilon_\phi$  for the 15 dSphs in Table 1. From this table we can find that the dSphs which have the same  $J_{\text{obs}}$  may have different values of  $J_S$ , for instance, Carina and Hercules. The  $V_{\text{max}}$  and  $R_{V_{\text{max}}}$  for these dSphs are not the same, thus leads to a different dark matter particle velocity distribution. To see

how the J-factor uncertainty impacts on the constraints of the dark matter annihilation cross section, we calculate  $\mathcal{L}_i(\boldsymbol{\mu}, \boldsymbol{\theta}_i | \mathcal{D}_i)$  with  $J_i = J_{\text{obs},i}$  and take it as the total likelihood (here the annihilation cross section is velocity-independent). We can then determine the regions of the annihilation cross section excluded at 95% confidence level performing a test statistic, comparing the likelihood with and without the dark matter signal. In Figure 7 we show our calculation results (solid lines) and compare them with the constraints given by the Fermi Collaboration (dot line). As we can see, the constraints that do not take the J-factor likelihood into account may be more stringent than the Fermi results at most 2% – 5%, and the discrepancies go to zero at large dark matter masses.

Following the above procedures, we determine the constraints on  $\varepsilon_\phi$  at 95% confidence level as a function of dark matter mass, the results are shown in Figure 8. As shown in the figure, all of the  $\varepsilon_\phi$  parameter space has been excluded for the dark matter mass  $m_\chi \lesssim 100$  GeV, since the Fermi-LAT experiment has the ability to detect the dark matter signal with a cross section below the canonical thermal relic cross section in this region. As expected, the constraints from the dSphs searching results are much more stringent than that from the subhalo observation results. In Figure 9, we also show the constraints on the dark matter annihilation cross section at 95% confidence level for given Sommerfeld-enhanced J-factors. We firstly calculate the Sommerfeld-enhanced J-factor with the given particle parameters  $\varepsilon_\phi$  and  $\alpha_X$  for each dwarf galaxy, and then we calculate the signal gamma-ray flux from dark matter annihilation for each choice of dark matter annihilation cross section. Following the same procedures, we determine the 95% confidence level upper limits on the dark matter annihilation cross section. The coupling  $\alpha_X$  is assumed to be 0.1 here, and we notice that the constraints are independent on this parameter for dark matter mass  $m_\chi \lesssim 10$  TeV. As shown in the figure, our results highlight that the Sommerfeld enhancement hypothesis is discordant with the WIMPs scenario, these results are in line with the previous studies [35, 79].

The anomaly in the cosmic positron fraction data at energies  $\gtrsim 10$  GeV has motivated dark matter candidates with Sommerfeld-enhanced annihilations. Comprehensive analysis to the AMS-02 experiment  $e^+/(e^- + e^+)$  data show that the required enhancement is in the range of  $\sim (200 - 2000)$  and the dark matter mass is in the range of  $\sim (700 - 2500)$  GeV [45]. In the left panel of Figure 10, we show the results of Sommerfeld enhancement with various coupling  $\alpha_X$ . The dark matter particle velocity is taken to be 220 km/s which is a typical value for the Galactic dark matter. As shown in the figure, to reach the required enhancement we should require a large coupling to the light force carrier,  $\alpha_X \gtrsim 0.1$ . We then fix the coupling  $\alpha_X$  at 0.1 and randomly generate the parameters points with  $\varepsilon_\phi$  in  $10^{-2} - 1$  and dark matter mass in the range of  $(700 - 2500)$  GeV. We pick out the points that produce a Sommerfeld enhancement  $S > 150$ . Through these procedures we estimate the parameter space that may account for the AMS-02 positron fraction anomaly, the results are shown by the green bands in the right panel of Figure 10. The constraint from the Fermi-LAT dSphs searches is represented by the red line, these results clear show that the Sommerfeld enhancement parameter spaces that may account for the AMS-02 positron anomaly have already been excluded by the Fermi-LAT gamma-ray observation results.

## 6 Summary

In the case of velocity-independent dark matter cross section, J-factor is independent of the underlying dark matter particle physics and can be simply factorized from the particle physics. However, for the case of velocity-dependent dark matter cross section, the cross sec-

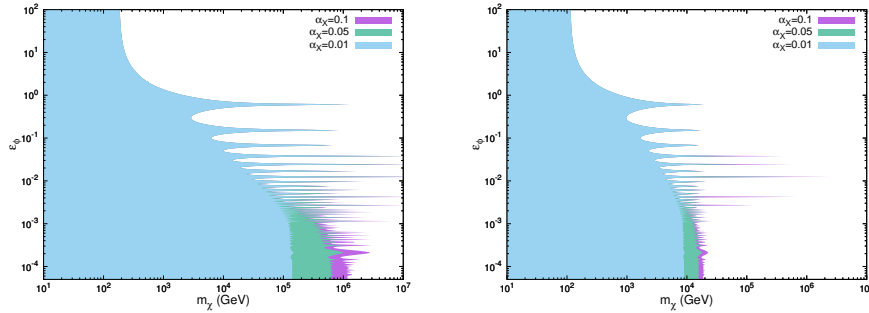


**Figure 8.** The Fermi-LAT dSphs searches constrain on the  $\epsilon_\phi$  at 95% confidence level. The color shaded parameter space is excluded at 95% confidence level, the dark matter annihilation channel is assumed to be  $b\bar{b}$  and  $\tau\bar{\tau}$  in the left and right panel.

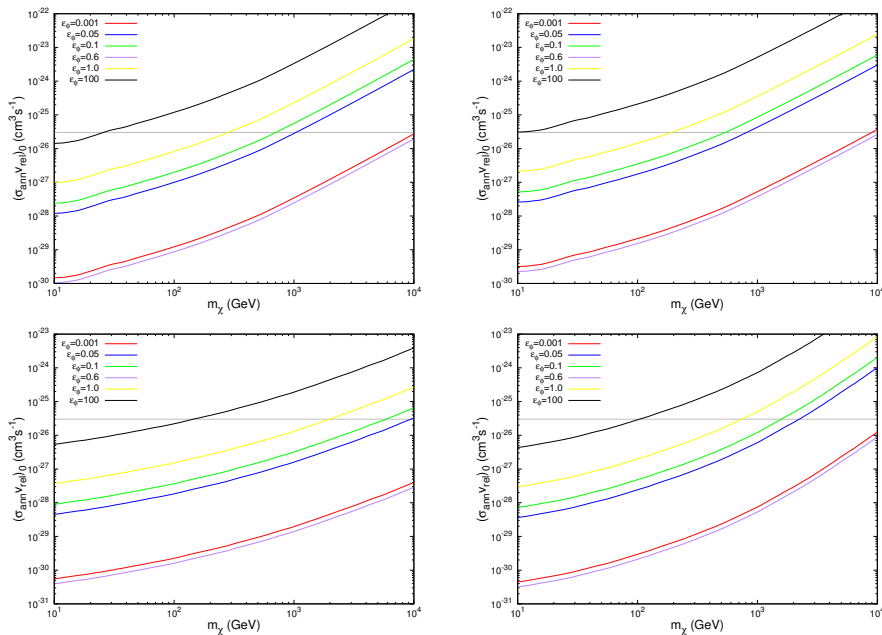


**Figure 9.** Constraints on the dark matter annihilation cross section at 95% confidence level derived from the Fermi-LAT dSphs searches, with a given Sommerfeld-enhanced J-factor. The horizontal grey line stands for a annihilation cross section  $(\sigma_{\text{ann}} v_{\text{rel}})_0 = 3 \times 10^{-26} \text{ cm}^3 \text{ s}^{-1}$ , the dark matter annihilation channel is assumed to be  $e^+e^-$ ,  $\mu^+\mu^-$ ,  $b\bar{b}$  and  $\tau\bar{\tau}$  from the upper left panel to the lower right panel.

tion cannot be extracted from the J-factor directly, since the photon flux arising from dark matter annihilation depends on the dark matter velocity distribution. In this work we focus on the dark matter annihilation cross section that is enhanced by the Sommerfeld effect. We determine the dark matter velocity distribution for the NFW dark matter density profile using the Eddington's formula, with the assumption that the orbits of dark matter particles are isotropic. We define a dimensionless dark matter velocity distribution function and show that this distribution function can be well fitted by a exponential form of velocity. We then calculate the Sommerfeld-enhanced J-factor with the dark matter velocity distribution function and show its behaviors in many parameter spaces. The subhalos and dSphs have low

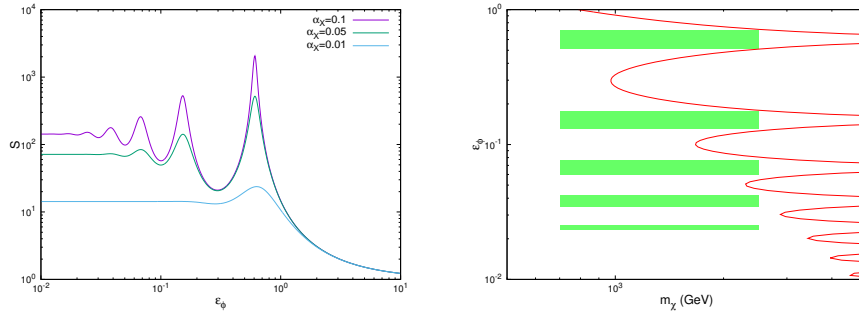


**Figure 10.** Left panel: Plots of Sommerfeld enhancement as a function of  $\varepsilon_\phi$  with various  $\alpha_X$ , assuming dark matter particle velocity  $v = 220$  km/s. Right panel: the green bands stand for the parameter points with the Sommerfeld enhancement  $S > 150$ , the red line represents the constraint from the Fermi-LAT dSphs observations.

characteristic dark matter particle velocities, thus are ideal sites to study the Sommerfeld enhancement effect. We use the Fermi-LAT gamma-ray sources observation results to put constraints on the Sommerfeld enhancement. For the subhalo observations, we count the number of sources that may be observed by the Fermi-LAT experiment and use this to determine the 95% confidence level Poisson upper limit on the predicted number of such sources. For the dSphs searches, we perform the analysis and use the likelihood function provided by the Fermi Collaboration to determine the constraints on the dark matter parameters space at 95% confidence level. Fitting to the AMS-02 positron fraction data show that to account for the positron anomaly with dark matter scenario, the required enhancement and dark matter mass is in the range  $(200 - 2000)$  and  $(700 - 2500)$  GeV. However, our results show that these parameter spaces have already been excluded by the Fermi-LAT gamma-ray observation results. Our results may also put stringent constraints on the self-interacting dark matter models that may account for the Galactic Center GeV gamma-ray excess.

## Acknowledgments

This work is supported in part by the National Key Research and Development Program of China No. 2017YFA0402200 and 2017YFA0402204, the NSFC under Grants No. 11335012 and No. 11475237, and the Key Research Program of Frontier Sciences, CAS.

## A Dimensionless velocity distribution function

The NFW density profile can be expressed in the scaled form

$$\rho(r) = \rho_s \times \tilde{\rho}(\tilde{r}), \quad (\text{A.1})$$

where  $\tilde{\rho}$  is a dimensionless quantity as a function of  $\tilde{r} = r/r_s$ . Then the gravitational potential can be written as

$$\Psi(r) = G\rho_s r_s^2 \times \tilde{\Psi}(\tilde{r}), \quad (\text{A.2})$$

where the dimensionless gravitational potential is given by

$$\tilde{\Psi}(\tilde{r}) = \begin{cases} -C/\tilde{r}_{\max} - 4\pi \int_{\tilde{r}}^{\tilde{r}_{\max}} (\ln(1 + \tilde{r}) - \tilde{r}/(1 + \tilde{r}))/\tilde{r}^2 d\tilde{r} & \text{if } \tilde{r} < \tilde{r}_{\max} \\ -C/\tilde{r} & \text{if } \tilde{r} \geq \tilde{r}_{\max} \end{cases} \quad (\text{A.3})$$



with  $C = 4\pi(\ln(1 + \tilde{r}_{\max}) - \tilde{r}_{\max}/(1 + \tilde{r}_{\max}))$  and  $\tilde{r}_{\max} = 2.163$ . We can also define a dimensionless energy per unity mass

$$\tilde{\varepsilon} = \tilde{v}^2/2 + \tilde{\Psi}(\tilde{r}), \quad (\text{A.4})$$

where  $\tilde{v} = (G\rho_s r_s^2)^{-1/2}v$  is a dimensionless velocity. With these dimensionless quantities, the dark matter distribution function can be written as

$$f(\varepsilon) = \rho_s (G\rho_s r_s^2)^{-3/2} \tilde{f}(\tilde{\varepsilon}), \quad (\text{A.5})$$

where  $\tilde{f}(\tilde{\varepsilon})$  is the dimensionless dark matter velocity distribution function, which has the same form as eq.(2.1)

$$\tilde{f}(\tilde{\varepsilon}) = \frac{1}{\sqrt{8\pi^2}} \int_{\tilde{\varepsilon}}^0 \frac{d^2\tilde{\rho}}{d\tilde{\Psi}^2} \frac{d\tilde{\Psi}}{\sqrt{\tilde{\Psi} - \tilde{\varepsilon}}}. \quad (\text{A.6})$$

We find this dimensionless dark matter velocity distribution function can be parameterized as

$$\tilde{f}(\tilde{r}, \tilde{v}) = \exp\left(\sum_{n=0}^{\infty} a_n(\tilde{r})\tilde{v}^n\right), \quad (\text{A.7})$$

where  $a_n(\tilde{r})$  is a coefficient that depends on the dimensionless radius  $\tilde{r}$ . The series n expands to 5 or 6 can give well fitting results with this formula. We show the numerical and fitting results of dimensionless distribution function  $\tilde{f}(\tilde{r}, \tilde{v})$  in Figure 11. The purple lines in the figure represent the numerical results and the green lines stands for the fitting results, from the upper left panel to the lower right panel the “radius”  $\tilde{r}$  are set at 0.1, 0.5, 1.0 and 1.5 respectively. As shown in the figure, the dimensionless distribution function  $\tilde{f}(\tilde{r}, \tilde{v})$  is nearly a constant when “velocity”  $\tilde{v} \lesssim 0.1$ , while drops rapidly to zero as “velocity” increasing. The figure also shows that dimensionless distribution function  $\tilde{f}(\tilde{r}, \tilde{v})$  decreases with the increasing of “radius”.

## B Analytic solutions for the Sommerfeld enhancement

In the limit of a massless force carrier, the Yukawa potential becomes a Coulomb potential and can be solved analytically [27]. In this case the Sommerfeld enhancement factor is given by

$$S = \frac{\pi/\varepsilon_v}{1 - e^{-\pi/\varepsilon_v}}. \quad (\text{B.1})$$

In the low-velocity regime  $v \ll \alpha_X$ ,  $S \simeq \pi\alpha_X/v$ . There are no resonances in the Sommerfeld enhancement for the Coulomb case, because the potential is not localized. We notice that the  $1/v$  behavior breaks down at very small velocities [61]. To see this, we can expand the Yukawa potential in powers of  $y = m_\phi r$

$$V(r) \simeq -\frac{\alpha_X}{r}(1 - m_\phi r) = V_c(r)(1 - m_\phi r), \quad (\text{B.2})$$

where  $V_c(r)$  is the Coulomb potential. The radial Schrödinger equation becomes

$$\frac{1}{m_\chi}\psi''(r) - V_c(r)\psi(r) = -(m_\chi v^2 - m_\phi\alpha)\psi(r). \quad (\text{B.3})$$

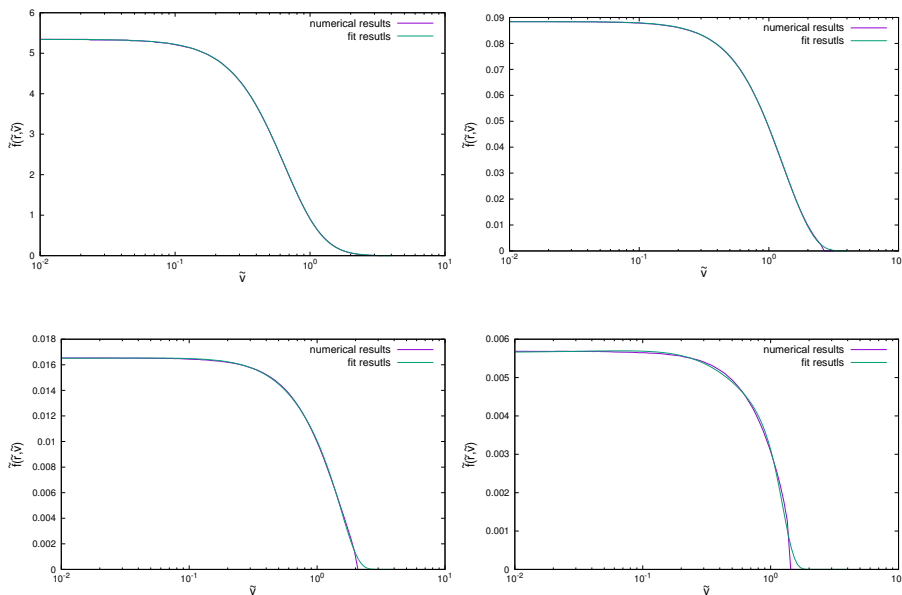


**Figure 11.** Numerical and fitting results of dimensionless velocity distribution function  $\tilde{f}(\tilde{r}, \tilde{v})$  as a function  $\tilde{r}$ . The “radius”  $\tilde{r}$  is set at 0.1 and 0.5 for the upper two panels, and for the lower two panels the “radius”  $\tilde{r}$  is set at 1.0 and 1.5 respectively.

The Coulomb case can be recovered by the Yukawa case when the condition  $v^2 \gg m_\phi \alpha_X / m_\chi$  holds. The Sommerfeld enhancement saturates at low velocity for a nonzero mass of mediator  $\phi$ . Since the attractive force has a finite range  $\sim 1/m_\phi$ , the Sommerfeld enhancement saturates at  $S \sim 1/\varepsilon_\phi$  when the deBroglie wavelength of the particle  $1/(m_\chi v)$  gets larger than the interaction range [37].

The analytic solution for the Schrödinger equation can also be possible by approximating the Yukawa potential as the Hulthén potential [62, 63], and the resulting Sommerfeld enhancement is given by

$$S = \frac{\pi}{\varepsilon_v} \frac{\sinh\left(\frac{2\pi\varepsilon_v}{\pi^2\varepsilon_\phi/6}\right)}{\cosh\left(\frac{2\pi\varepsilon_v}{\pi^2\varepsilon_\phi/6}\right) - \cos\left(2\pi\sqrt{\frac{1}{\pi^2\varepsilon_\phi/6} - \frac{\varepsilon_v^2}{(\pi^2\varepsilon_\phi/6)^2}}\right)}. \quad (\text{B.4})$$

The analytic result is an excellent approximation, typically reproducing the numerical results to within fractional differences of 10%, while in the resonance regions, the discrepancies may be as large as a factor of 2 or beyond [35, 49]. We show the analytic approximation (green lines) and numerical results (purple lines) of the Sommerfeld enhancement in Figure 12.

## References

- [1] G. Jungman, M. Kamionkowski and K. Griest, *Supersymmetric dark matter*, *Phys. Rept.* **267** (1996) 195 [hep-ph/9506380].
- [2] L. Bergström, *Nonbaryonic dark matter: observational evidence and detection methods*, *Rept. Prog. Phys.* **63** (2000) 793 [hep-ph/0002126].
- [3] G. Bertone, D. Hooper and J. Silk, *Particle dark matter: evidence, candidates and constraints*, *Phys. Rept.* **405** (2005) 279 [hep-ph/0404175].

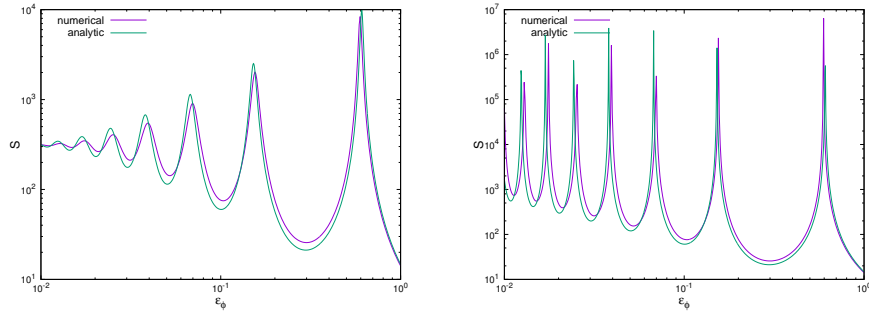


**Figure 12.** Numerical and analytic solutions of the Sommerfeld enhancement factor  $S$  as a function of  $\varepsilon_\phi$ , evaluated at  $\varepsilon_v = 10^{-2}$  (left panel) and  $\varepsilon_v = 10^{-4}$  (right panel) respectively.

- [4] B. W. Lee and S. Weinberg, *Cosmological lower bound on heavy-neutrino masses* *Phys. Rev. Lett.* **39** (1977) 165.
- [5] P. Hut, *Limits on masses and number of neutral weakly interacting particles* *Phys. Lett.* **69B** (1977) 85.
- [6] T. Bringmann and C. Weniger, *Gamma ray signals from dark matter: concepts, status and prospects*, *Phys. Dark Univ.* **1** (2012) 194 [arXiv:1208.5481].
- [7] M. Klasen, M. Pohl and G. Sigl, *Indirect and direct search for dark matter*, *Prog. Part. Nucl. Phys.* **85** (2015) 1 [arXiv:1507.03800].
- [8] D. Merritt, M. Milosavljevic, L. Verde and R. Jimenez, *Dark matter spikes and annihilation radiation from the galactic center*, *Phys. Rev. Lett.* **88** (2002) 191301 [astro-ph/0201376].
- [9] A. Cesarini, F. Fucito, A. Lionetto, A. Morselli and P. Ullio, *The Galactic Center as a dark matter gamma-ray source*, *Astropart. Phys.* **21** (2004) 267 [astro-ph/0305075].
- [10] S. Dodelson, D. Hooper and P. D. Serpico, *Extracting the gamma ray signal from dark matter annihilation in the galactic center region*, *Phys. Rev. D* **77** (2008) 063512 [arXiv:0711.4621].
- [11] F. Stoehr et al., *Dark matter annihilation in the halo of the Milky Way*, *Mon. Not. Roy. Astron. Soc.* **345** (2003) 1313 [astro-ph/0307026].
- [12] L. Bergström, P. Ullio and J. H. Buckley, *Observability of gamma-rays from dark matter neutralino annihilations in the Milky Way halo*, *Astropart. Phys.* **9** (1998) 137 [astro-ph/9712318].
- [13] G. Bertone, A. R. Zentner and J. Silk, *A new signature of dark matter annihilations: gamma-rays from intermediate-mass black holes*, *Phys. Rev. D* **72** (2005) 103517 [astro-ph/0509565].
- [14] P. Brun, G. Bertone, J. Lavalle, P. Salati and R. Taillet, *Antiproton and positron signal enhancement in dark matter mini-spikes scenarios*, *Phys. Rev. D* **76** (2007) 083506 [arXiv:0704.2543].
- [15] T. Bringmann, J. Lavalle and P. Salati, *Intermediate mass black holes and nearby dark matter point sources: a myth-buster*, *Phys. Rev. Lett.* **103** (2009) 161301 [arXiv:0902.3665].
- [16] P. A. R. Ade et al., *Planck 2015 results. XIII. Cosmological parameters*, *Astron. Astrophys.* **594** (2016) A13 [arXiv:1502.01589].
- [17] S. D. M. White and C. S. Frenk, *Galaxy formation through hierarchical clustering*, *Astrophys. J.* **379** (1991) 52.
- [18] C. S. Frenk and S. D. M. White, *Dark matter and cosmic structure*, *Annalen Phys.* **524** (2012) 507 [arXiv:1210.0544].

- [19] Á. Moliné, M. A. Sánchez-Conde, S. Palomares-Ruiz and F. Prada, *Characterization of subhalo structural properties and implications for dark matter annihilation signals*, *Mon. Not. R. Astron. Soc.* **466** (2017) 4 [arXiv:1603.04057].
- [20] M Ackermann et al., *Search for dark matter satellites using Fermi-LAT*, *Astrophys. J.* **747** (2012) 121 [arXiv:1201.2691].
- [21] C. Boehm, T. Ensslin and J. Silk, *Can Annihilating dark matter be lighter than a few GeVs?*, *J. Phys. G* **30** (2004) 279 [astro-ph/0208458].
- [22] C. Boehm and P. Fayet, *Scalar dark matter candidates*, *Nucl. Phys. B* **683** (2004) 219 [hep-ph/0305261].
- [23] C Boehm, D Hooper, J Silk, M Casse, J Paul, MeV dark matter: Has it been detected?, *Phys. Rev. Lett.* **92** (2004) 101301 [arXiv:astro-ph/0309686].
- [24] B. E. Robertson and A. R. Zentner, *Dark matter annihilation rates with velocity dependent annihilation cross sections*, *Phys. Rev. D* **79** (2009) 083525 [arXiv:0902.0362].
- [25] A. Alves, S. Profumo, F. S. Queiroz and W. Shepherd, *Effective field theory approach to the Galactic Center gamma-ray excess*, *Phys. Rev. D* **90**, 115003 (2014).
- [26] S. Profumo and W. Shepherd, *Pitfalls of dark matter crossing symmetries* *Phys. Rev. D* **88**, 056018 (2013) [arXiv:1307.6277].
- [27] A. Sommerfeld, *Ann. Phys. (Leipzig)* **403** (1931) 257.
- [28] S. Profumo, *TeV  $\gamma$ -rays and the largest masses and annihilation cross sections of neutralino dark matter*, *Phys. Rev. D* **72** (2005) 103521 [arXiv:astro-ph/0508628].
- [29] J. Hisano, M. Nagai, M. Nojiri and M. Senami, *Explosive dark matter annihilation*, *Phys. Rev. Lett.* **92** (2004) 031303 [arXiv:hep-ph/0307216].
- [30] J. Hisano, S. Matsumoto, M. Nojiri and S. Saito, *Nonperturbative effect on dark matter annihilation and gamma ray signature from the galactic center*, *Phys. Rev. D* **71**, 063528 (2005) [arXiv:hep-ph/0412403].
- [31] M. Cirelli, A. Strumia and M. Tamburini, *Cosmology and astrophysics of minimal dark matter*, *Nucl. Phys.* **B787**, 152 (2007) [arXiv:0706.4071 [hep-ph]].
- [32] J. M. Russell, S. M. West, D. Cumberbatch and D. Hooper, *Heavy dark matter through the Higgs portal*, *J. High Energy Phys.* **07** (2008) 058.
- [33] M. Pospelov and A. Ritz, *Astrophysical signatures of secluded dark matter*, *Phys. Lett.* **B671**, 391 (2009).
- [34] J. L. Feng, M. Kaplinghat and H. B. Yu, *Halo-Shape and Relic-Density Exclusions of Sommerfeld-Enhanced Dark Matter Explanations of cosmic-ray Excesses*, *Phys. Rev. Lett.* **104** (2010) 151301 [arXiv:0911.0422].
- [35] J. L. Feng, M. Kaplinghat and H. B. Yu, *Sommerfeld enhancements for thermal relic dark matter*, *Phys. Rev. D* **82** (2010) 083525 [arXiv:1005.4678].
- [36] J. Zavala, M. Vogelsberger, S. D. M. White, *Relic density and CMB constraints on dark matter annihilation with Sommerfeld enhancement*, *Phys. Rev. D* **81** (2010) 083502 [arXiv:0910.5221].
- [37] N. A. Hamed, D. P. Finkbeiner, T. R. Slatyer and N. Weiner, *A Theory of Dark Matter*, *Phys. Rev. D* **79** (2009) 015014 [arXiv:0810.0713].
- [38] Z. P. Liu, Y. L. Wu and Y. F. Zhou, *Sommerfeld enhancements with vector, scalar, and pseudoscalar force carriers*, *Phys. Rev. D* **88** (2013) 096008 [arXiv:1305.5438].
- [39] PAMELA collaboration, O. Adriani et al., *An anomalous positron abundance in cosmic-rays with energies 1.5-100 GeV*, *Nature* **458** (2009) 607 [arXiv:0810.4995].

- [40] AMS collaboration, M. Aguilar et al., *First Result from the Alpha Magnetic Spectrometer on the International Space Station: Precision Measurement of the Positron Fraction in Primary cosmic-rays of 0.5-350 GeV*, *Phys. Rev. Lett.* **110** (2013) 141102.
- [41] L. Bergström, J. Edsjö and G. Zaharijas, *Dark matter interpretation of recent electron and positron data*, *Phys. Rev. Lett.* **103** (2009) 031103 [arXiv:0905.0333].
- [42] A. Ibarra, A. S. Lamperstorfer and J. Silk, *Dark matter annihilations and decays after the AMS-02 positron measurements*, *Phys. Rev. D* **89** (2014) 063539 [arXiv:1309.2570].
- [43] M. Di Mauro, F. Donato, N. Fornengo, R. Lineros and A. Vittino, *Interpretation of AMS-02 electrons and positrons data*, *J. Cosm. Astropart. Phys.* **04** (2014) 006 [arXiv:1402.0321].
- [44] G. Giesen et al., *AMS-02 antiprotons, at last! Secondary astrophysical component and immediate implications for Dark Matter*, *J. Cosm. Astropart. Phys.* **09** (2015) 023.
- [45] H. B. Jin, Y. L. Wu and Y. F. Zhou, *Implications of the first AMS-02 measurement for dark matter annihilation and decay*, *J. Cosm. Astropart. Phys.* **11** (2013) 026 [arXiv:1304.1997].
- [46] Q. Yuan et al., *Implications of the AMS-02 positron fraction in cosmic-rays*, *Astropart. Phys.* **60** 2015 1-12 [arXiv:1304.1482].
- [47] J. Chen and Y. F. Zhou, *The 130 GeV gamma-ray line and Sommerfeld enhancements*, *J. Cosm. Astropart. Phys.* **1304** (2013) 017 [arXiv:1301.5778].
- [48] F. Ferrer and D. R. Hunter, *The impact of the phase-space density on the indirect detection of dark matter*, *J. Cosm. Astropart. Phys.* **09** (2013) 005 [arXiv:1306.6586].
- [49] K. K. Boddy, J. Kumar, L. E. Strigari, *M. Y. Wang Sommerfeld-Enhanced J-Factors For Dwarf Spheroidal Galaxies*, *Phys. Rev. D* **95** (2017) 123008 [arXiv:1702.00408].
- [50] D. J. R. Campbell et al., *Knowing the unknowns: uncertainties in simple estimators of galactic dynamical masses*, *Mon. Not. Roy. Astron. Soc.* **469** (2017) 2 [arXiv:1603.04443].
- [51] J. Binney and S. Tremaine, *Galactic Dynamics: Second Edition*, Princeton University Press, Princeton U.S.A. (2008).
- [52] V. Bonnavard et al., *Dark matter annihilation and decay in dwarf spheroidal galaxies: the classical and ultrafaint dSphs*, *Mon. Not. Roy. Astron. Soc.* **453** (2015) 849 [arXiv:1504.02048].
- [53] J. F. Navarro, C. S. Frenk and S. D. White, *A Universal density profile from hierarchical clustering*, *Astrophys. J.* **490** (1997) 493 [astro-ph/9611107].
- [54] M. Kuhlen, M. Vogelsberger and R. Angulo, *Numerical Simulations of the Dark Universe: State of the Art and the Next Decade*, *Phys. Dark Univ.* **1** (2012) 50 [arXiv:1209.5745].
- [55] J. Diemand and B. Moore, *The structure and evolution of cold dark matter halos*, *Adv. Sci. Lett.* **4** (2011) 297 [arXiv:0906.4340].
- [56] W. de Blok, *The Core-Cusp Problem*, *Adv. Astron.* **2010** (2010) 789293 [arXiv:0910.3538].
- [57] D. N. Spergel and P. J. Steinhardt, *Observational evidence for self-interacting cold dark matter*, *Phys. Rev. Lett.* **84** (2000) 3760 [arXiv:astro-ph/9909386].
- [58] M. Kaplinghat, S. Tulin and H. B. Yu, *Dark Matter Halos as Particle Colliders: Unified Solution to Small-Scale Structure Puzzles from Dwarfs to Clusters*, *Phys. Rev. Lett.* **116** (2016) 041302 [arXiv:1508.03339].
- [59] S. Tulin, H. B. Yu and K. M. Zurek, *Resonant Dark Forces and Small-Scale Structure*, *Phys. Rev. Lett.* **110** (2013) 111301 [arXiv:1210.0900].
- [60] A. Kamada, M. Kaplinghat, A. B. Pace and H. B. Yu *Self-Interacting Dark Matter Can Explain Diverse Galactic Rotation Curves*, *Phys. Rev. Lett.* **119** (2017) 111102 [arXiv:1611.02716].
- [61] M. Lattanzi, *Can the WIMP annihilation boost factor be boosted by the Sommerfeld enhancement?*, *Phys. Rev. D* **79** (2009) 083523 [arXiv:0812.0360].

- [62] S. Cassel, *Sommerfeld factor for arbitrary partial wave processes*, *J. Phys. G* **37** (2010) 105009 [arXiv:0903.5307].
- [63] T. R. Slatyer, *The Sommerfeld enhancement for dark matter with an excited state*, *J. Cosmol. Astropart. Phys.* **02** (2010) 028 [arXiv:0910.5713].
- [64] B. Q. Lu and H. S. Zong, *Limits on dark matter from AMS-02 antiproton and positron fraction data*, *Phys. Rev. D* **93** (2016) 103517 [arXiv:1510.04032].
- [65] G. D. Martinez, *A Robust Determination of Milky Way Satellite Properties using hierarchical mass modelling* *Mon. Not. Roy. Astron. Soc.* **451** (2015) 2524 [arXiv:1309.2641].
- [66] A. G. Sameth, S. M. Koushiappas and M. Walker, *DWARF GALAXY ANNIHILATION AND DECAY EMISSION PROFILES FOR DARK MATTER EXPERIMENTS* *Astrophys. J.* **801** (2015) 74 [arXiv:1408.0002].
- [67] J. L. Sanders, N. W. Evans, A. G. Sameth and W. Dehnen, *Indirect Dark Matter Detection for Flattened Dwarf Galaxies* *Phys. Rev. D* **94** (2016) 063521 [arXiv:1604.05493].
- [68] N. W. Evans, J. L. Sanders and A. Geringer-Sameth, *Simple J-Factors and D-Factors for Indirect Dark Matter Detection* *Phys. Rev. D* **93** (2016) 103512 [arXiv:1604.05599].
- [69] Fermi-LAT collaboration, A. A. Abdo et al., *Fermi large area telescope first source catalog*, *Astrophys. J. Suppl.* **188** (2010) 405-436 [arXiv:1002.2280].
- [70] Fermi-LAT collaboration, F. Acero et al., *Fermi Large Area Telescope third source catalog*, *Astrophys. J. Suppl.* **218** (2015) 23 [arXiv:1501.02003].
- [71] A. Berlin and D. Hooper, *Stringent constraints on the dark matter annihilation cross section from subhalo searches with the Fermi Gamma-Ray Space Telescope*, *Phys. Rev. D* **89** (2014) 016014 [arXiv:1309.0525].
- [72] B. Bertoni, D. Hooper and T. Linden Examining, *The Fermi-LAT Third Source Catalog in search of dark matter subhalos*, *J. Cosmol. Astropart. Phys.* **12** (2015) 035 [arXiv:1504.02087].
- [73] D. Hooper and S. J. Witte, *Gamma Rays From Dark Matter Subhalos Revisited: Refining the Predictions and Constraints*, *J. Cosmol. Astropart. Phys.* **04** (2017) 018 [arXiv:1610.07587].
- [74] J. Diemand et al., *Clumps and streams in the local dark matter distribution*, *Nature* **454** (2008) 735738, [arXiv:0805.1244].
- [75] S. G. Kimmel, M. Boylan-Kolchin, J. Bullock and K. Lee, *ELVIS: Exploring the Local Volume in Simulations*, *Mon. Not. Roy. Astron. Soc.* **438** (2014) 25782596, [arXiv:1310.6746].
- [76] N. Gehrels, *Confidence limits for small numbers of events in astrophysical data*, *Astrophys. J.* **303** (1986) 336.
- [77] Fermi-LAT collaboration, M. Ackermann et al., *Searching for Dark Matter Annihilation from Milky Way Dwarf Spheroidal Galaxies with Six Years of Fermi Large Area Telescope Data*, *Phys. Rev. Lett.* **115** (2015) 231301.
- [78] Fermi-LAT collaboration, M. Ackermann et al., *Dark matter constraints from observations of 25 Milky Way satellite galaxies with the Fermi Large Area Telescope*, *Phys. Rev. D* **89** (2014) 042001 [arXiv:1310.0828].
- [79] T. Bringmann and P. Walia *Strong Constraints on Self-Interacting Dark Matter with Light Mediators*, *Phys. Rev. Lett.* **118** (2017) 141802 [arXiv:1612.00845].